

Extensible and Scalable Adaptive Sampling on Supercomputers

Eugen Hruska,^{1,2} Vivekanandan Balasubramanian,³ John R. Ossyra,⁴ Shantenu Jha,³ and Cecilia Clementi^{1,5,2,*}

¹*Center for Theoretical Biological Physics, Rice University, Houston, TX, United States*

²*Department of Physics, Rice University, Houston, TX, United States*

³*Department of Electrical and Computer Engineering,
Rutgers University, Piscataway, NJ 08854, USA*

⁴*University of Tennessee/Oak Ridge National Laboratory,
Center for Molecular Biophysics, Oak Ridge, TN, USA*

⁵*Department of Chemistry, Rice University, Houston, TX, United States*

(Dated: May 17, 2022)

The accurate sampling of protein dynamics is an ongoing challenge despite the utilization of High Performance Computers (HPC) systems. Utilizing only "brute force" MD simulations requires an unacceptably long time to solution. Adaptive sampling methods allow a more effective sampling of protein dynamics than standard MD simulations. Depending on the restarting strategy the speed up can be more than one order of magnitude. One challenge limiting the utilization of adaptive sampling by domain experts is the relatively high complexity to efficiently running it on HPC systems. We discuss how the ExTASY framework can set up new adaptive sampling strategies, and reliably execute resulting workflows at scale on HPC platforms. Here the folding dynamics of three small proteins is predicted with no a priori information.

I. INTRODUCTION

Molecular dynamics (MD) simulations with all-atom force-fields allow simulating protein folding and protein kinetics with good accuracy. Reaching biologically relevant processes, such as protein folding or drug binding, is limited mainly by the required large computational resources and long simulation times. The long simulation times can be reduced either by simulating parallel trajectories with massively-distributed computing [1, 2] or with special-purpose hardware [3]. Further reduction of required computational resources or simulation times would allow a more broad application of MD simulations.

One method of reducing both the computational resources and the simulation times is *adaptive sampling* [4–15]. Adaptive sampling is an iterative process, where MD simulations from previous iterations are analyzed, and, based on the analysis, a new iteration of relatively short MD trajectories is initiated. The starting conformations for the MD trajectories are determined in such a way to efficiently reach a goal such as crossing rare transitions barriers, folding a protein, or recovering the dynamics of a macromolecule. The exact strategy where to restart new MD simulations determines the success of the adaptive sampling approach, and several different methods have been proposed and investigated [7–10, 15–19]. Adaptive sampling requires to use multiple parallel simulations and is therefore suitable for High Performance Computers (HPC).

Determining the efficiency, accuracy and reliability of a particular adaptive sampling strategy is challenging for several reasons. Different proteins can behave differently for different adaptive sampling strategies but limited computational resources don't allow to adaptively

sample a statistically significant number of proteins with different strategies for comparison. Accurate results are known only for a limited number of proteins. Despite these challenges some performance analyses of adaptive sampling strategies have been performed [5–8, 15]. The results show that some adaptive sampling strategies are both reliable, accurate and reach speed ups of one or more orders of magnitude with respect to "brute force" MD. The larger, more complex the protein the higher speed up is expected [15].

An important challenge in adaptive sampling simulations is the complexity of performing the required computational tasks efficiently on HPC platforms with heterogeneous software and hardware environments. This complexity can detract from the core objective of investigating the behavior of a particular protein or the efficiency of new adaptive sampling strategies. Some of the existing frameworks which currently strive to reduce this entry-barrier to adaptive sampling, such as HTMD[9] and SSAGES [20], are either bound to specific software packages, algorithms, computing platforms or are not open source. In contrast, the ExTASY[21] framework is not coupled to specific software packages, supports multiple adaptive sampling algorithms and is extensible, to new algorithms and methods, while being open source and agnostic of the HPC platform. In addition to demonstration of the scientific results that can be achieved by using ExTASY, in this manuscript, we investigate the advantages of scalability, reliability or reproducibility arising from ExTASY framework for adaptive sampling.

II. METHODS

Many different implementations of adaptive sampling exist but they all have in common that the previous MD simulations are analysed and restart points for the next

* cecilia@rice.edu

batch of MD simulations are determined from the analysis of the sampled configurational space. The different implementations mainly differ in the analysis step, and they can be based on Markov State Models (MSMs) [22–26], Diffusion Maps [27–30], likelihood-based approaches [31], cut-based free energy profiles [32], or neural networks [33–35]. In this manuscript, we exemplify the usage of the ExTASY framework with Markov State Models with different restarting strategies, as described in Section II B.

A. Adaptive Sampling

In each iteration of Markov State Models-based adaptive sampling, all previous MD simulations are analysed. Figure 1 is a graphical representation of the process. In the first iteration of the adaptive sampling, the MD simulations are generated from the system starting state as shown in Step 1.

In Step 2 all previous trajectories are analysed. In the case of Markov State Models-based adaptive sampling used here, a dimension reduction with Time-lagged Independent Component Analysis (TICA) [36, 37] converts the raw trajectories in low-dimensional trajectories. The Koopman method [38–43] is used to reduce the non-equilibrium effects emerging from collecting many short MD trajectories. The resulting low-dimensional trajectories are scaled into a kinetic map [44, 45], which provides a measure of the kinetic distance between different configurations. The kinetic map is then clustered with k-means into approximately 200 microstates, the detailed values for each protein are provided in the Supplementary Information. A maximum-likelihood estimation with a detailed balance constraint [22] allows to obtain an MSM transition matrix between every pair of microstates. The value of the lag time parameter, τ , for the TICA analysis and for the MSM was chosen based on the results of [46], which compared and optimized the parameter selection for the proteins simulated here. All the analysis was performed using the PyEMMA Python package [47], which allows fast adjustments in the analysis step. The exact parameters for the MSM construction for each protein are listed in the Supplementary Information. All these steps can be modified or replaced easily in the ExTASY workflow.

The overall adaptive sampling process described in Figure 1 can be summarized as follows:

- **Start:** Start with a start conformation. In the cases presented here, we start from a configuration in the unfolded state of a protein.
- **Step 1:** Generate a batch of molecular dynamics trajectories from the selected conformations, the parallelisation is defined by the available computational resources. This step is described in Section II E.

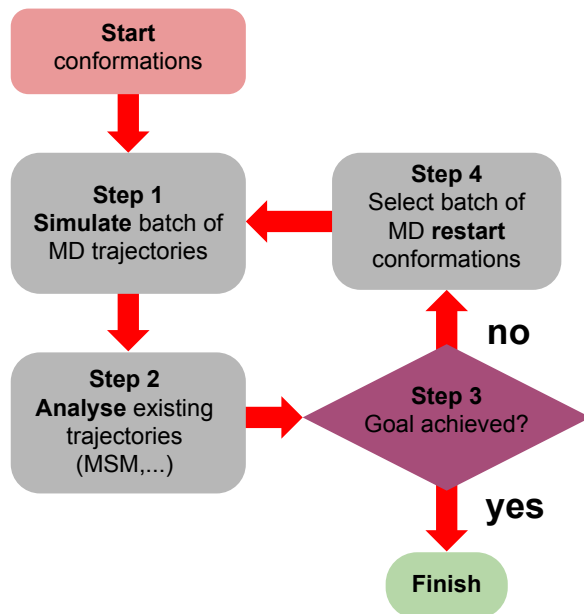


FIG. 1: The flow chart shows the basic structure of adaptive sampling. The number of starting conformations is variable. The software and hardware to generate the MD simulations are variable. Different Analysis methods in Step 2 are possible, commonly TICA [36, 37] and MSM [22] are used, but alternative methods such as Vampnet [33] are possible. In Step 3 the goal can be also variable, from finding the whole protein dynamics to exploring smaller-scale changes. Step 4 allows different adaptive sampling strategies such as the FAST method [19] or the strategies discussed in this work.

- **Step 2:** Analyse the all available data as described in Section II A, using the probabilities from the MSM transition matrix.
- **Step 3:** Decide if the goal of adaptive sampling is achieved. In this work, the goal is finding the folded state and obtaining a converged equilibrium dynamics for the protein. If the goal is not achieved, proceed to Step 4; otherwise, stop the iterative process.
- **Step 4:** Select the batch of protein conformations for Step 1 in the next iteration as described in Section II B.

After Step 2 the adaptive sampling continues with Step 4 if the goal is not achieved. This goal could be folding the protein, achieving a pre-determined accuracy of the protein dynamics, but could also be manually set to finish after a number of iterations. If the goal is not achieved in Step 3, in Step 4 a batch of protein conformations for the next iteration is selected as described in Section II B. If the goal in Step 3 is achieved, the iterative adaptive sampling finishes and the trajectories can be further analysed.

B. Restart Strategies for Adaptive Sampling

In the ExTASY framework, the different Restart Strategies in Step 4 in Figure 1 are easily exchangeable. Here we use two strategies, the first one is the Macrostate Count based strategy, further called *cmacro* strategy, and the second one is the Microstate Count based strategy, further called *cmicro* strategy. The *cmacro* strategy was shown to be more effective in reaching the folded state of the protein and the *cmicro* strategy was shown to be more effective in exploring the whole protein landscape [15]. To benefit from the different strengths of the two strategies we use in this implementation the *cmacro* strategy in the initial iterations for each protein, until the folded state is reached; then we continue the iterations with the *cmicro* strategy to improve the accuracy of the protein dynamics. These two strategies do not assume any a priori knowledge of the system except the chemical structure of the unfolded protein, but other adaptive sampling strategies which use additional information about the protein can be used in the ExTASY framework.

a. Adaptive sampling strategy cmicro One simple restart strategy is starting new molecular dynamics trajectories in the microstates which have the worse statistics, that is, that have been visited the least during prior iterations [6, 7, 9, 10]. This statement can be quantified by using the counts in the count matrix of the MSM from Step 2, that report on how many times all previous trajectories have visited each microstate. The probability that any given microstate is selected in Step 4 for the batch of restart conformations is inversely proportional to its associated count. This strategy is less effective to fold a protein than the *cmacro* strategy (described below), so in this work the *cmicro* is only employed after the folded state is found. The *cmicro* strategy is more effective to explore new regions of the whole protein landscape and to better sample the protein dynamics [15].

b. Adaptive sampling strategy cmacro Another popular restart strategy for adaptive sampling is a macrostate-based method indicated here as *cmacro*. The main advantage of this method is the faster folding of proteins or crossing of transition barriers [15]. This advantage is achieved by using eigenvectors of the on-the-fly MSM from Step 2 to select more restart configurations in areas which are kinetically disconnected or less explored. In this method, the microstates of the on-the-fly MSM are clustered into macrostates, for example with PCCA [48]. Any microstate not connected in the main MSM is treated as an additional macrostate. The number of macrostates can be either fixed, as in this work, or determined based on the number of slow processes emerging from the analysis. The macrostate count is determined by measuring how many times any previous trajectory has visited each macrostate. The restart conformations for the next iteration of adaptive sampling are then chosen from each macrostate inversely proportional to the macrostate count. Individual conformations

within a macrostate are selected inversely proportional to the microstate count within the macrostate.

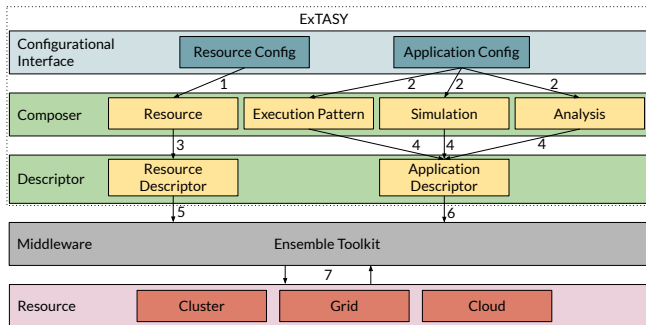


FIG. 2: ExTASY-EnTK Integration: The diagram illustrates the seven execution steps of an adaptive sampling algorithm using ExTASY.

C. Tools and Software

ExTASY is a domain specific workflow system [49, 50] for adaptive sampling algorithms on HPC platforms. ExTASY exposes domain specific parameters and simulation configurations, but abstracts complexities of execution management, resource acquisition and management using RADICAL-Cybertools (RCT) [51]. RCTs are software systems designed and implemented in accordance with the building blocks approach [50]. Each system is independently designed with well-defined entities, functionalities, states, events and errors. Specifically, ExTASY uses Ensemble Toolkit (EnTK) [52] and RADICAL-Pilot (RP) [53]. Ensemble Toolkit [52, 54] provides the ability to create and execute ensemble-based applications with complex coordination and communication but without the need for explicit resource management. EnTK uses RP [53], which provides resource management and task execution capabilities. In this section, we describe the ExTASY framework and how it leverages capabilities offered by EnTK and RP.

1. ExTASY

ExTASY exposes configuration files to interface with users and two components: Composer and Descriptor.

The Composer validates the user input and creates the Resource, Execution Pattern, Simulation, and Analysis sub-components. The Resource represents a valid resource description; Execution Pattern describes the number of iterations, number of simulation tasks per iteration and number of analysis tasks per iteration; Simulation and Analysis describe the parameters to be used for simulation and analysis tasks.

The Descriptor interfaces with Ensemble Toolkit, the execution middleware. It consists of two sub-

```

from radical.entk import Task, Stage, Pipeline
p = Pipeline()

sim_stage = Stage()
sim_task = Task()
sim_task.executable = <executable> #example
openmm
sim_task.arguments = <args> #example openmm args
<add other task properties>
sim_stage.add_tasks(sim_task)

ana_stage = Stage()
ana_task = Task()
ana_task.executable = <executable> #example
pyemma
ana_task.arguments = <args> #example pyemma args
<add other task properties>

ana_stage.add_tasks(ana_task)
ana_stage.post_exec = {
    'condition': eval_sims(),
    'on_true':   add_sims(),
    'on_false':  terminate()
}

p.add_stages([sim_stage, ana_stage])

```

FIG. 3: Pseudocode describing the adaptive sampling algorithm using the EnTK API

components: Resource Descriptor and Application Descriptor. The former converts the resource description to a format as accepted by the middleware. The latter uses the information from the Execution Pattern, Simulation and Analysis sub-components to describe the complete application to be executed.

Figure 2 presents the integration between ExTASY and the execution middleware (EnTK). ExTASY translates the adaptive sampling application into ordered executable tasks through a series of events: ExTASY parses the configurational files to determine parameters to be used and creates Resource description (event 1) and the simulation and analysis tasks to be executed (event 2). ExTASY then uses EnTK’s interface to describe the resource and application (event 3 and 4) and initiate execution on the target resource (event 5 and 6). EnTK executes all the simulations and analysis on the resource (event 7).

ExTASY uses EnTK programming abstractions and EnTK’s application programming interface (API). ExTASY also uses EnTK’s capabilities to support adaptive execution [55] by modifying the execution plan depending upon intermediate results e.g., add more simulations and analysis tasks. Figure 3 provides pseudo-code on how ExTASY implements an adaptive sampling algorithm using the EnTK API.

2. Ensemble Toolkit & RADICAL-Pilot

EnTK simplifies the creation and execution of applications with complex ensemble coordination and communication requirements. EnTK decouples the description

of ensemble coordination and communication from their execution by separating three distinct concerns: (i) specification of task and resource requirements; (ii) resource acquisition and management; and (iii) task execution.

EnTK enables the encoding of ensemble applications by exposing an API with four components: Application Manager, Pipeline, Stage and Task. Users specify their application using pipelines, stages, and tasks. Users then pass this specification and description of the target resource to the Application Manager. Resource description includes properties like wall-time, number of nodes and credentials for resource access.

The Task component is used to encapsulate an executable and its software environment. The Stage component contains a set of tasks without mutual dependencies and that can therefore be executed concurrently. The Pipeline component is used to describe a sequence of stages. Description of ensemble applications in terms of concurrency and sequentiality avoids the need to explicitly specify dependencies between tasks.

EnTK supports an explicit definition of pre and post conditions on the execution of tasks, enabling fine-grained adaptivity [55]. Adaptivity allows modifications to the number, type and order of tasks to be executed during runtime, based on intermediate results. Specifically, EnTK supports three types of adaptivity: (i) adaptivity in the number of tasks; (ii) adaptivity in the order of tasks; and (iii) adaptivity in the properties of a task.

EnTK provides a simple programming model, abstracts the complexities of resource and execution management, and adds only a small and well-bounded overhead on the execution of $O(1000)$ tasks [52]. EnTK uses a runtime system, such as RADICAL-Pilot, to acquire the resources needed, manage task execution, as well as provide portability across heterogeneous HPC resources.

RADICAL-Pilot: Two methods traditionally used to execute multiple HPC tasks are: (i) each task is scheduled as an individual job; or (ii) use message-passing interface (MPI) capabilities to execute multiple tasks as part of a single job. The former method requires each task to be independently executed; the latter method is suboptimal for heterogeneous or interdependent tasks. The pilot abstraction [56] addresses some of these limitations. The pilot abstraction: (i) uses a placeholder job without any tasks assigned to it, so as to acquire resources; and, (ii) decouples the initial resource acquisition from task-to-resource assignment. Once the pilot is scheduled tasks are scheduled within its spatio-temporal resource boundaries, which allows computational tasks to be executed directly without being queued. The pilot abstraction thus supports the requirements of task-level parallelism and high-throughput, while respecting queue policies and constraints of HPC batch scheduling. RADICAL-Pilot is an implementation of the pilot abstraction, engineered to support scalable and efficient launching of heterogeneous tasks across different platforms.

D. Reference Data

To show the speed up and accuracy of the adaptive sampling method we compared the results with preexisting long MD simulations of 3 small proteins, obtained on the Anton supercomputer [57]. These proteins and the reference data were investigated before [46, 58], allowing us to demonstrate here the usefulness and reliability of the ExTASY workflow. The 3 proteins are summarized in Table I, their size is 10 to 35 residues and the folding time within a few μ s. These proteins were chosen due to their folding time which is long enough to show the advantages of adaptive sampling with ExTASY framework, but still reachable with our computational resources. Only the C-alpha coordinates are used when comparing the reference data trajectories with the results from the ExTASY framework in this work.

TABLE I: Adaptively sampled proteins in this study

Protein	PDB ID	# Residues	Folding Time (μ s) [57]	Unfolding Time (μ s)
Chignolin	5AWL	10	0.6	2.2
Villin	2F4K	35	2.8	0.9
BBA	1FME	28	18	5

E. Molecular dynamics simulation

The MD simulations in this work were performed with OpenMM 7.0.1 [59] using CUDA 7.5 on the Blue Waters supercomputer. To reproduce the same setup as in [57] we used CHARMM22* force field [60] and the modified TIP3P water. The stepsize used was 5fs, and the trajectories were strided to match the 0.2 ns stepsize of the reference data. Differently from [57], we used the Particle Mesh Ewald method for long-range electrostatics due to OpenMM limitations. The protein Start states at the beginning of the adaptive sampling were selected randomly from the 20% of frames with the highest Root Mean Square Deviation (RMSD) from the corresponding crystal structure. A short energy equilibration (1-2ns) was then performed in the NPT ensemble to create initial coordinates for the workflows. No further a priori information was given to the ExTASY framework except the unfolded start conformations.

In each iteration 50 OpenMM trajectories were simulated on 50 XK nodes on Blue Waters with one node per trajectory. The length of each trajectory was 50ns for Chignolin and Villin and 100ns for BBA. ExTASY was used for each of the three proteins, using a total of 150 nodes at the same time. ExTASY scales to greater number of nodes, so can be used to simulate even larger proteins, or more proteins concurrently. Steps 2 and 4 were performed on one node on Blue Waters utilizing the same job on Blue Waters as the MD simulations (Step 1). A job length of 48h was chosen on Blue Waters to maximize the number of iterations executed in each job. After all the simulations are finished, the folding times,

speed up and the accuracy of protein dynamics was determined by comparing with the Anton MD simulations starting from the selected start conformation.

III. RESULTS AND DISCUSSION

In order to analyse the efficiency of adaptive sampling, we considered several measures. To show the completeness of the exploration, we measured the fraction of explored population and considered the overlap of the explored areas with the reference dataset. This also allows us to estimate the speed up time to solution compared to the reference method. To analyse the accuracy of the simulated protein dynamics we compare the relative entropy of the MSM transition matrices, and the Mean First Passage Time (MFPT) to the folded state, as detailed below.

A. Comparison of Exploration

The whole explored energy landscape of the protein cannot be visualized due to the high dimensionality of the raw trajectories, but the explored landscape in the reduced TICA coordinates is shown in Figure 4. The colored background shows the explored free energy landscape of the reference dataset and the shaded foreground shows the region of this landscape explored by the adaptive sampling. It is clear that the whole energy landscape of the three proteins is explored by ExTASY. The small differences in Figure 4 could be caused by the difference in the long-range electrostatics setup.

To show how effectively the whole protein landscape is explored, we use the fraction of the total population explored as a function of time. Here we select all the states which are explored at a certain time and compare with all possible states (as obtained from the reference simulations). To represent the different importance of different states we weight the explored states with their stationary weight. The population of each microstate is calculated as the stationary weight of that microstate from the MSM analysis of the reference dataset. Figure 5 reports the comparison of the explored populations as a function of time for the reference dataset and the ExTASY results, and shows that for all three proteins the ExTASY exploration is about 1 order of magnitude faster than the reference. The x-axis in Figures 5-7 is absolute simulation time to show the improvement of time to solution with ExTASY. Absolute simulation time is the length of one trajectory in Step 1 times the number of iterations. When all the trajectories in Step 1 are run in parallel, the absolute simulation time shows the time to solution independent of the used hardware. The effects of parallelisation on the time to solution for adaptive sampling was explored in [15], generally both adaptive sampling and parallelisation decrease the time to solution.

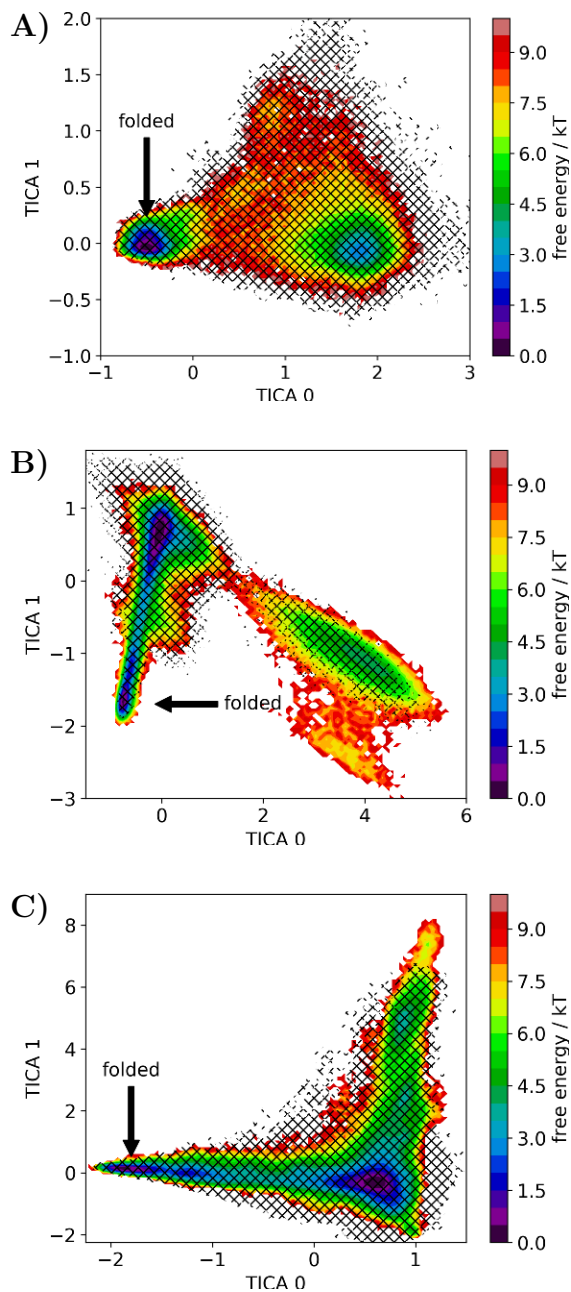


FIG. 4: Exploration of the protein energy landscape in TICA coordinates. The color background shows the explored Free Energy landscape by the reference dataset. The black diagonal lines on top show the explored conformations by the adaptive sampling in this paper. The almost perfect overlap shows that the whole conformational landscape of the three proteins was explored. The label shows the location of the folded state. Individual proteins: A) Chignolin B) Villin C) BBA

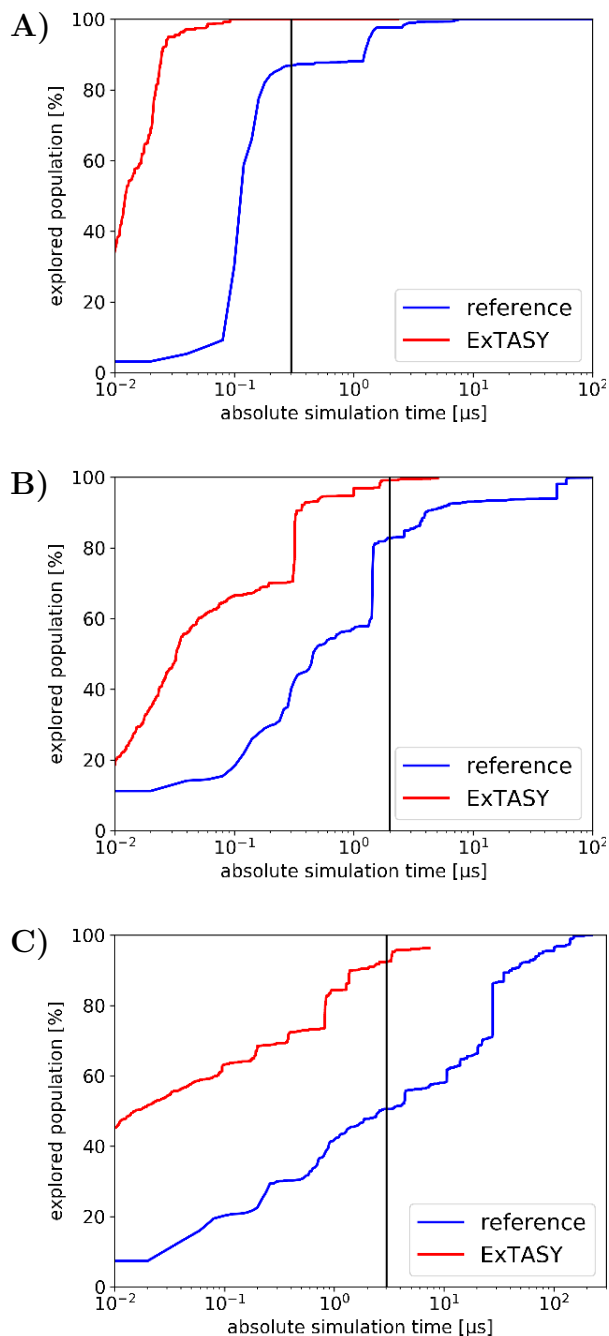


FIG. 5: The population of explored states evolving with absolute simulation time. Around one order of magnitude shorter time to solution can be reached with adaptive sampling compared to "brute force" MD simulations. The black vertical line shows the change between the implementation of the *macro* adaptive strategy for the initial iterations (left of the black line) and the *micro* adaptive strategy (right of the black line), described in Section II B. Individual proteins: A) Chignolin B) Villin C) BBA

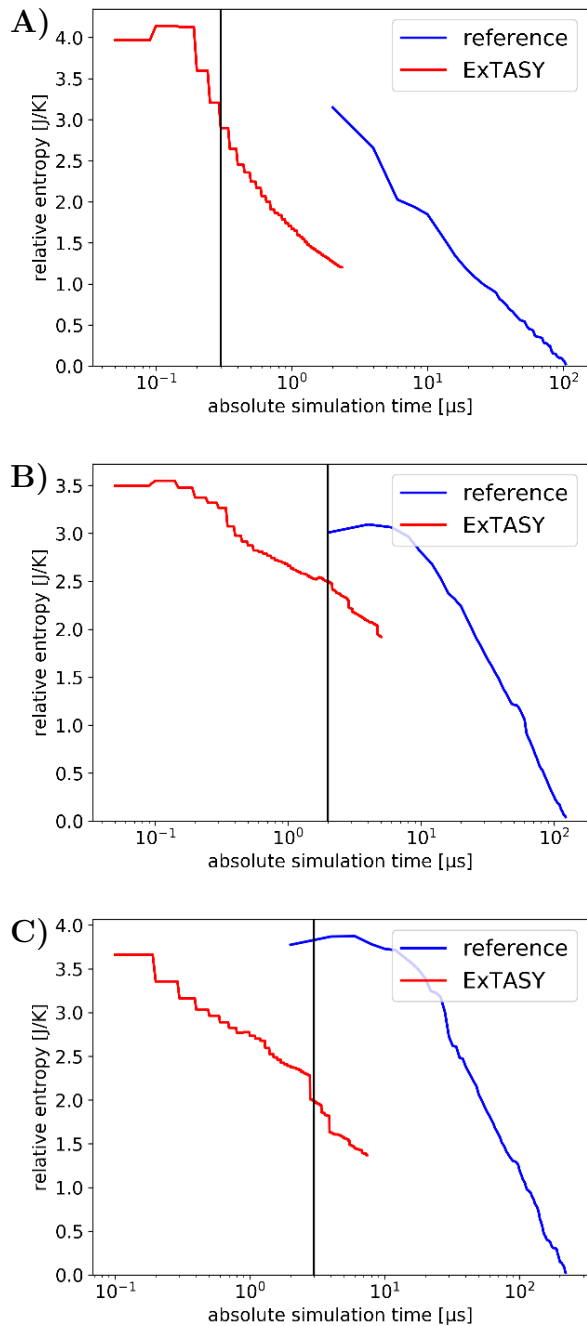


FIG. 6: Relative entropy between the MSM transition matrices generated during the ExTASY exploration and from the reference data. Results for individual proteins: A) Chignolin B) Villin C) BBA. The relative entropy decreases with increasing number of adaptive sampling iterations. For iteration on the left of the black vertical line, the *macro* adaptive strategy was implemented, while on the right of the black line the *micro* adaptive strategy was implemented (see Section II B).

B. Comparison of Protein Dynamics

To track the convergence of protein dynamics in the adaptive sampling workflow, one can use the relative entropy [5] between the MSM transition matrix of the reference data, P_{ij} , and the MSM transition matrix of the analysed data, Q_{ij} . A relative entropy can be calculated between each microstate in the analysed and the reference transition probabilities from this state. By averaging the relative entropy for each state weighted by the stationary probability over all microstates we obtain the relative entropy between the two transition matrices. The relative entropy $D(P||Q)$ is then given by

$$D(P||Q) = \sum_{i,j}^N s_i P_{ij} \ln \frac{P_{ij}}{Q_{ij}}. \quad (1)$$

where s_i is the equilibrium probability of state i . The transition matrices P_{ij} and Q_{ij} have to use exactly the same dimension reduction and same clustering. As zero counts in the transition matrices can cause divergence of the relative entropy, a pseudo-count of $1/N$ (where N is the length of the simulation) is added to each element of the count matrices before normalizing the rows to get the transition matrices [5]. Figure 6 shows how the relative entropy decreases with increasing simulation time. The relative entropy of the reference trajectory is obtained by using the reference data up to the specified simulation time. By definition, the relative entropy of the full reference trajectory is zero. Analogously the relative entropy for the ExTASY simulation data is obtained from the data up to the specified simulation time. In Figure 6 we observe a rapid decrease of both the reference relative entropy and ExTASY relative entropy. At the same absolute simulation time ExTASY shows a smaller relative entropy compared to the reference data.

Figure 7 shows how the Mean First Passage Time (MFPT) from the unfolded to the folded state converges as a function of simulation time, for the adaptive sampling and reference simulations. The final MFPT obtained with the two methods are comparable. These results are similar to what was obtained with the HTMD framework [9]. One possible reason for the minor discrepancies in MFPT between the results from ExTASY adaptive sampling and the reference data is the difference in the treatment of electrostatic.

The folded and unfolded areas of the proteins for the MFPT calculation were defined by the RMSD relative to the PDB crystal structures (reported in Table I). The threshold values for the individual proteins can be found in the Supplementary Information.

IV. CONCLUSION

We have shown that the ExTASY framework [21] can effectively perform adaptive sampling, as exemplified with different adaptive exploration strategies. The

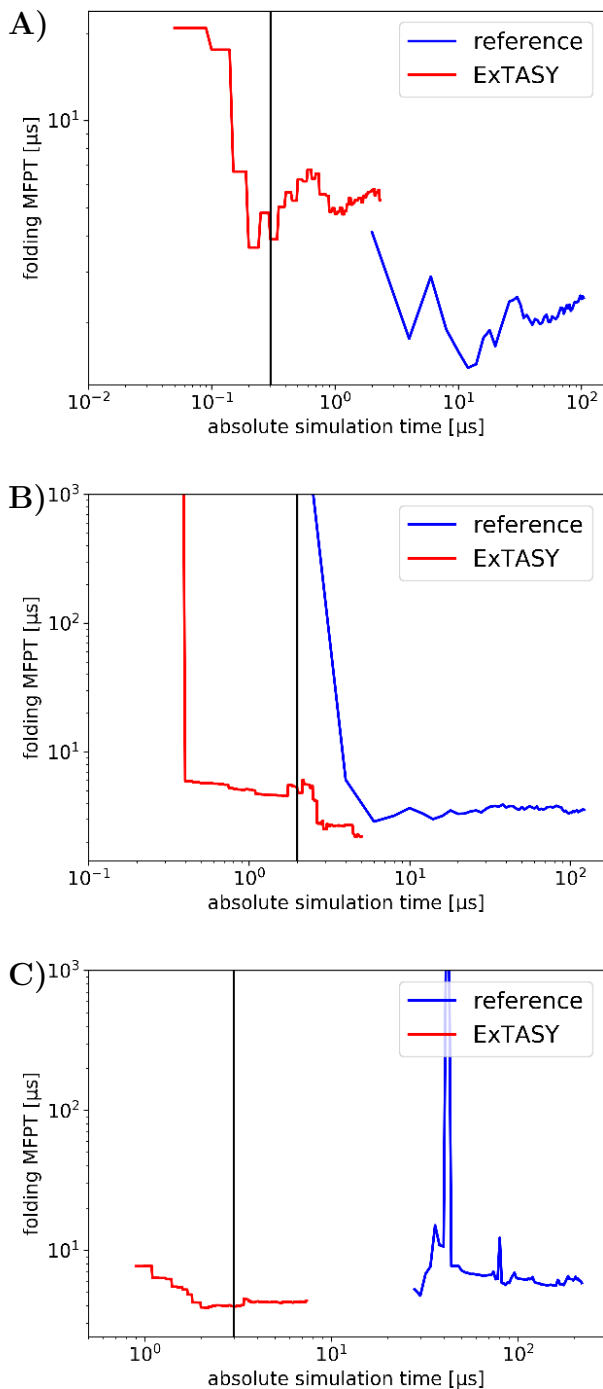


FIG. 7: Mean first passage time (MFPT) from unfolded to folded states evolving as more data is available after more adaptive sampling iterations. The blue lines show MFPT from the reference data. Two different adaptive sampling strategies are used, *macro* until the black vertical line and *micro* after the black line, as described in Section II B. Individual proteins: A) Chignolin B) Villin C) BBA

whole free energy landscape of the 3 proteins selected for this study was efficiently explored. The speed up compared to "brute force" molecular dynamics simulation was about one order of magnitude. The MFPT folding times converged to values similar to the reference values and the relative entropy between the transition matrix of the MSM computed during the adaptive sampling and the MSM of the reference simulations decreases steadily with the simulation time.

The ExTASY framework reduces the time spent by domain experts in executing adaptive sampling in a scalable fashion on diverse platforms. Due to the design and implementation of the ExTASY framework [21], it can be easily modified for different proteins or MD simulation software. It can also be easily extended to different adaptive sampling strategies and platforms. All the code used in this work is available at <https://github.com/ClementiGroup/ExTASY>.

V. SUPPLEMENTARY MATERIALS

See Supplementary material for the ExTASY workflow parameters and more results for the 3 proteins.

ACKNOWLEDGMENTS

We thank D.E. Shaw Research for the reference dataset of Molecular Dynamics trajectories. This work is supported in part by the National Science Foundation (CHE-1265929, CHE-1740990, CHE-1900374, and PHY-1427654 to C.C.), the Welch Foundation (C-1570 to C.C.). Supercomputing time was provided by Blue Waters (supported by the National Science Foundation (awards OCI-0725070 and ACI-1240993) sustained-petascale computing project via NSF 1713749.

-
- [1] M. Shirts and V. S. Pande, *Science* **290**, 1903 (2000).
- [2] I. Buch, M. J. Harvey, T. Giorgino, D. P. Anderson, and G. De Fabritiis, *J. Chem. Inf. Model* **50**, 397 (2010).
- [3] D. E. Shaw, J. Grossman, J. A. Bank, B. Batson, J. A. Butts, J. C. Chao, M. M. Deneroff, R. O. Dror, A. Even, C. H. Fenton, *et al.*, in *Proceedings of the international conference for high performance computing, networking, storage and analysis* (IEEE Press, 2014) pp. 41–53.
- [4] N. Singhal and V. S. Pande, *J. Chem. Phys.* **123**, 204909 (2005).
- [5] G. R. Bowman, D. L. Ensign, and V. S. Pande, *J. Chem. Theory Comput.* **6**, 787 (2010).
- [6] J. K. Weber and V. S. Pande, *J. Chem. Theory Comput.* **7**, 3405 (2011).
- [7] S. Doerr and G. De Fabritiis, *J. Chem. Theory Comput.* **10**, 2064 (2014).
- [8] J. Preto and C. Clementi, *Phys. Chem. Chem. Phys.* **16**, 19181 (2014).
- [9] S. Doerr, M. Harvey, F. Noé, and G. De Fabritiis, *J. Chem. Theory Comput.* **12**, 1845 (2016).
- [10] D. Lecina, J. F. Gilabert, and V. Guallar, *Sci. Rep.* **7**, 8466 (2017).
- [11] Z. Shamsi, A. S. Moffett, and D. Shukla, *Sci. Rep.* **7**, 12700 (2017).
- [12] M. I. Zimmerman and G. R. Bowman, *J. Chem. Theory Comput.* **11**, 5747 (2015).
- [13] B. Trendelkamp-Schroer and F. Noé, *Phys. Rev. X* **6**, 011009 (2016).
- [14] N. Plattner, S. Doerr, G. De Fabritiis, and F. Noé, *Nat. Chem.* **9**, 1005 (2017).
- [15] E. Hruska, J. R. Abella, F. Nüske, L. E. Kavrakli, and C. Clementi, *J. Chem. Phys.* **149** (2018).
- [16] A. Dickson and C. L. Brooks, *J. Phys. Chem. B* **118**, 3532 (2014).
- [17] M. C. Zwier, J. L. Adelman, J. W. Kaus, A. J. Pratt, K. F. Wong, N. B. Rego, E. Suárez, S. Lettieri, D. W. Wang, M. Grabe, D. M. Zuckerman, and L. T. Chong, *J. Chem. Theory Comput.* **11**, 800 (2015).
- [18] A. Z. Guo, E. Sevgen, H. Sidky, J. K. Whitmer, J. A. Hubbell, and J. J. de Pablo, *J. Chem. Phys.* **148** (2018).
- [19] M. I. Zimmerman, J. R. Porter, X. Sun, R. R. Silva, and G. R. Bowman, *JCTC* **12**, 5459 (2018).
- [20] H. Sidky, Y. J. Colón, J. Helfferich, B. J. Sikora, C. Bezik, W. Chu, F. Giberti, A. Z. Guo, X. Jiang, J. Lequieu, J. Li, J. Moller, M. J. Quevillon, M. Rahimi, H. Ramezani-Dakhel, V. S. Rathee, D. R. Reid, E. Sevgen, V. Thapar, M. A. Webb, J. K. Whitmer, and J. J. de Pablo, *J. Chem. Phys.* **148** (2018).
- [21] V. Balasubramanian, I. Bethune, A. Shkurti, E. Breitmoser, E. Hruska, C. Clementi, C. Laughton, and S. Jha, *Proceedings of the 2016 IEEE 12th International Conference on e-Science*, 361 (2016).
- [22] J.-H. Prinz, H. Wu, M. Sarich, B. Keller, M. Senne, M. Held, J. D. Chodera, C. Schütte, and F. Noé, *J. Chem. Phys.* **134**, 174105 (2011).
- [23] B. E. Husic and V. S. Pande, *J. Am. Chem. Soc.* **140**, 2386 (2018).
- [24] G. R. Bowman, V. Pande, and F. Noé, in *Advances in Experimental Medicine and Biology*, Vol. 797 (Springer, 2014).
- [25] N.-V. Buchete and G. Hummer, *J. Phys. Chem. B* **112**, 6057 (2008).
- [26] C. Schütte, A. Fischer, W. Huisinga, and P. Deuffhard, *J. Comp. Phys.* **151**, 146 (1999).
- [27] R. R. Coifman, S. Lafon, A. B. Lee, M. Maggioni, B. Nadler, F. Warner, and S. W. Zucker, *Proc. Natl. Acad. Sci. USA* **102**, 7426 (2005).
- [28] M. A. Rohrdanz, W. Zheng, M. Maggioni, and C. Clementi, *J. Chem. Phys.* **134**, 03B624 (2011).
- [29] W. Zheng, B. Qi, M. A. Rohrdanz, A. Caffisch, A. R. Dinner, and C. Clementi, *J. Phys. Chem. B* **115**, 13065 (2011).
- [30] L. Boninsegna, G. Gobbo, F. Noé, and C. Clementi, *J. Chem. Theory Comput.* **11**, 5947 (2015).
- [31] B. Peters and B. L. Trout, *J. Chem. Phys.* **125**, 054108 (2006).
- [32] S. V. Krivov and M. Karplus, *Proc. Natl. Acad. Sci. USA* **105**, 13841 (2008).
- [33] A. Mardt, L. Pasquali, H. Wu, and F. Noé, *Nat. Comm.* **9** (2018).
- [34] C. Wehmeyer and F. Noé, *J. Chem. Phys.* **148**, 241703 (2018).
- [35] J. M. L. Ribeiro, P. Bravo, Y. Wang, and P. Tiwary, *J. Chem. Phys.* **149** (2018).
- [36] G. Pérez-Hernández, F. Paul, T. Giorgino, G. De Fabritiis, and F. Noé, *J. Chem. Phys.* **139**, 07B604_1 (2013).
- [37] C. R. Schwantes and V. S. Pande, *J. Chem. Theory Comput.* **9**, 2000 (2013).
- [38] B. O. Koopman, *Proc. Natl. Acad. Sci. USA* **17**, 315 (1931).
- [39] M. O. Williams, C. W. Rowley, and I. G. Kevrekidis, *J. Comput. Dynam.* **2**, 247 (2015).
- [40] M. O. Williams, I. G. Kevrekidis, and C. W. Rowley, *J. Nonlinear Sci.* **25**, 1307 (2015).
- [41] Q. Li, F. Dietrich, E. M. Bollt, and I. G. Kevrekidis, *Chaos* **27** (2017).
- [42] H. Wu, F. Nüske, F. Paul, S. Klus, P. Koltai, and F. Noé, *J. Chem. Phys.* **146**, 154104 (2017).
- [43] F. Nüske, H. Wu, J.-H. Prinz, C. Wehmeyer, C. Clementi, and F. Noé, *J. Chem. Phys.* **146**, 094104 (2017).
- [44] F. Noé and C. Clementi, *J. Chem. Theory Comput.* **11**, 5002 (2015).
- [45] F. Noé, R. Banisch, and C. Clementi, *J. Chem. Theory Comput.* **12**, 5620 (2016).
- [46] B. E. Husic, R. T. McGibbon, M. M. Sultan, and V. S. Pande, *J. Chem. Phys.* **145**, 194103 (2016).
- [47] M. K. Scherer, B. Trendelkamp-Schroer, F. Paul, G. Pérez-Hernández, M. Hoffmann, N. Plattner, C. Wehmeyer, J.-H. Prinz, and F. Noé, *J. Chem. Theory Comput.* **11**, 5525 (2015).
- [48] S. Röblitz and M. Weber, *Adv. Data. Anal. Classif.* **7**, 147 (2013).
- [49] M. Turilli, V. Balasubramanian, A. Merzky, I. Paraskevavakos, and S. Jha, *Computing in Science Engineering* **21**, 62 (2019).
- [50] M. Turilli, A. Merzky, V. Balasubramanian, and S. Jha, in *2018 18th IEEE/ACM International Symposium on Cluster, Cloud and Grid Computing (CCGRID)* (IEEE, 2018) pp. 348–349.
- [51] V. Balasubramanian, S. Jha, A. Merzky, and M. Turilli, “Radical-cybertools: Middleware building blocks for

- scalable science,” (2019), arXiv:1904.03085.
- [52] V. Balasubramanian, M. Turilli, W. Hu, M. Lefebvre, W. Lei, R. Modrak, G. Cervone, J. Tromp, and S. Jha, in *2018 IEEE International Parallel and Distributed Processing Symposium (IPDPS)* (IEEE, 2018) pp. 536–545.
- [53] A. Merzky, M. Turilli, M. Maldonado, M. Santcroos, and S. Jha, in *Workshop on Job Scheduling Strategies for Parallel Processing* (Springer, 2018) pp. 61–82.
- [54] V. Balasubramanian, A. Trekalis, O. Weidner, and S. Jha, in *Proceedings of the 45th International Conference on Parallel Processing (ICPP)* (2016) <http://arxiv.org/abs/1602.00678>.
- [55] V. Balasubramanian, T. Jensen, M. Turilli, P. Kasson, M. Shirts, and S. Jha, arXiv preprint arXiv:1804.04736 (2019).
- [56] M. Turilli, M. Santcroos, and S. Jha, *ACM Computing Surveys (CSUR)* **51**, 43 (2018).
- [57] K. Lindorff-Larsen, S. Piana, R. O. Dror, and D. E. Shaw, *Science* **334**, 517 (2011).
- [58] K. A. Beauchamp, R. McGibbon, Y.-S. Lin, and V. S. Pande, *Proc. Natl. Acad. Sci. USA* **44**, 17807 (2012).
- [59] P. Eastman, J. Swails, J. D. Chodera, R. T. McGibbon, Y. Zhao, K. A. Beauchamp, L.-P. Wang, A. C. Simonett, M. P. Harrigan, C. D. Stern, R. P. Wiewiora, B. R. Brooks, and V. S. Pande, *PLoS Comput. Biol.* **13**, e1005659 (2017).
- [60] S. Piana, K. Lindorff-Larsen, and D. E. Shaw, *Biophys. J.* **100** (2011).